J Solid State Electrochem (2012) 16:3097–3103
DOI 10.1007/s10008-012-1748-x

ORIGINAL PAPER

Electrochemical deposition of nanosemiconductor CuSe on multiwalled carbon nanotubes/polyimide membrane and photoelectric property researches

Jiajia Li · Huanhuan Kou · Yimin Jiang · Daban Lu · Zhixiang Zheng · Chunming Wang

Received: 4 January 2012 / Revised: 5 April 2012 / Accepted: 8 April 2012 / Published online: 27 April 2012

Abstract Nanosemiconductor CuSe were prepared on self-made multiwalled carbon nanotubes/polyimide (COOH-MWCNTs/PI) membrane electrode by electrochemical atomic layer deposition (EC-ALD). By exploring the elements, electrochemical properties through cyclic voltammetry and differential pulse-stripping voltammetry, -0.2 and -0.55 V are finally identified as the deposition potential of copper and selenium, respectively. Current density − time curve obtained via amperometric *I–t* processes indicates the formation of copper layer by a two-dimensional nucleation and growth mechanism, while selenium growth is considered to be diffusion control process. X-ray powder diffraction data reveals the preferred orientation of the CuSe crystal is at (112) plane. Field emission scanning electron microscopy and energy-dispersive X-ray spectroscopy analysis show that the obtained CuSe thin film are short virgate nanostructure, and the average atomic percentage of Cu:Se is close to one. Furthermore, the ultraviolet visible (UV–Vis) transmission measurements provide a band gap of 2.0 eV. Open-circuit potential (OCP) and amperometric *I–t* experiments illustrate the CuSe thin film to be p-type semiconductor. Obtained results indicate that the CuSe thin film depositing on COOH-CNTs/PI membrane is appropriate to serve as the solar energy transfer material.

Keywords CuSe · EC-ALD · COOH-CNTs/PI membrane · OCP · Solar cells

Electronic supplementary material The online version of this article (doi:10.1007/s10008-012-1748-x) contains supplementary material, which is available to authorized users.

J. Li · H. Kou · Y. Jiang · D. Lu · Z. Zheng · C. Wang (✉)
Department of Chemistry, Lanzhou University,
Lanzhou 730000, People's Republic of China
e-mail: wangcm@lzu.edu.cn

Introduction

Nowadays, I–VI binary compounds semiconductor have been widely used in the preparation of optical and photovoltaic devices [1, 2]. Among these materials, copper selenide (CuSe) have attracted broad attention and have been extensively studied in the past decades for they can served as the precursors of ternary polycrystalline Cu-chalcopyrites, such as $CuInSe_2$(CIS), $Cu(In,Ga)Se_2$ (CIGS). CuSe with nanostructure present a lot of potential applications in the fabrication of photovoltaic devices such as optical instruments, window material [3, 4], optical filter [5], solar cells [6–8], thermoelectric converter [9], and so on. CuSe have been synthetized with several methods such as chemical bath deposition (CBD) [10], solution phase reaction [11], vacuum evaporation, flash evaporation [12], electrodeposition [13, 14], and melting of Cu and Se [15], etc. It is proved that CuSe are typically p-type conductivity, with direct band gap close to 2.0 eV [16–18].

Electrochemical atomic layer deposition (EC-ALD), is a kind of electrochemical extending of atomic layer expiatory and atomic layer deposition, based on the underpotential deposition (UPD) of the elements that form the semiconductor compound in a cycle [19]. UPD is a name for an electrochemical surface-limited reaction, a phenomenon where an atomic layer of one element can form on a second element at a potential prior to, under, that needed to deposit the element on itself. In this work, we exploited a principle analogous to UPD to deposit a monolayer of one element on the CNT/PI electrode, which originated from the relatively strong adatom–substrate bond formed. Compared with other methods, electrodeposition is a low-cost, easily controlled, and convenient technique at ambient temperature; thus, it facilitates the formation of nanoparticle semiconductors, and the UPD principle makes it easier to control the monolayer based on the electrodeposition. Generally speaking, on an

appropriate substrate, in a suitable potential window, a potential scan can form a single layer of an element needed for semiconductor compound, multiple scans can form different element multilayers and different thickness of the element compound film [20]. Therefore, by adjusting the electrochemical parameter and electrolyte composition, it can be achieved to prepare different element compounds of certain ratio via EC-ALD method [21].

In the present study, we demonstrated that COOH-CNTs/PI membrane electrode could be effectively exploited for deposition of CuSe thin film by EC-ALD method through electrochemical properties research. The morphology, structural characterizations as well as photoelectrical properties of the materials were sketchily investigated. During the last decades, electrodeposition of CuSe has been intensively studied; however, to our best knowledge, there are rarely reports on the synthesis of CuSe with composite membrane serving as the substrate electrode. Herein, in this work, a new style substrate material (COOH-CNTs/PI composite membrane) was used, which showed good conductivity, excellent mechanical properties, stable performance between -250 and 300 °C temperature range, and light quality. These properties make COOH-CNTs/PI/CuSe materials useful for a variety of different applications of solar energy transfer material in extreme temperatures and the lighter quality condition, such as the spacecraft solar energy transfer material.

Experimental

4,4-Oxydianiline (ODA) and 4,4-oxydiphthalic anhydride (ODPA) were purchased from Shanghai Chemical (Shanghai, China). *N*-methyl pyrrolidone (NMP) was redistilled, multiwalled carbon nanotubes (MWCNTs) were purchased from Shenzhen Nanotech Port, which were conducted through oxidation treatment and ultrasonic processing to obtain carboxyl multiwalled carbon nanotubes (COOH-MWCNTs). $CuSO_4$, SeO_2, and other reagents were of analytical grade, and the solution were made up of water purified by Milli-Q pure water system (Millipore, electrical resistivity 18.2 MΩ/cm), and all the solutions were filled into high-purity N_2 to remove oxygen.

A CHI 832 electrochemical workstation (CH Instrument, USA) and a conventional three-electrode system were used in the experiments. The counter electrode was a platinum wire and a saturated calomel electrode (SCE) served as the reference electrode (all the potentials in this work will be referred to this SCE). The working electrode was self-made, which was made up of polyimide and COOH-MWCNTs. Firstly, appropriate amount of COOH-MWCNTs and anhydrous NMP were mixed together and stirred with an ultrasonic until a homogenous suspension of COOH-MWNT/NMP was obtained. Secondly, a 1:1 molar ratio of ODA and ODPA were added into anhydrous NMP solvent for 24 h in the magnetic stirrer to obtain polyamic acid (PAA). Lastly, the above two solutions were mixed uniformly and paved onto glass, then the slide was evaporated for 3 h at 60 °C, following heated up to 250 °C in 200 min, the COOH-MWCNTs/PI composite membrane was thus obtained. The electrolyzer for this pellet electrode designed in our laboratory was displayed in our former work [22].

The ingredient of the as-obtained films were identified via X-ray diffraction (XRD; RigakuD/Max-2400) data, the morphology of the material was viewed using field emission scanning electron microscopy (FE-SEM; Hitachi S-94 4800, Japan), the optical property was studied through UV–Vis (CARY 100Conc), CHI 832 electrochemical workstation with a 500 W xenon lamp (CHF-XM-500 W) was employed to study open-circuit potential (OCP) and amperometric *I–t* experiments.

For the thin film deposition, Cu was first deposited on the COOH-MWCNTs/PI membrane electrode; the aqueous solutions were: 5 mM $CuSO_4$ solution, pH 4.2, 0.2 M Na_2SO_4 served as supporting electrolyte. Then Se was deposited on Cu-covered COOH-MWCNTs/PI electrode; the aqueous solutions were: 5 mM H_2SeO_3 solution, pH 0.5, 0.1 M H_2SO_4 served as supporting electrolyte.

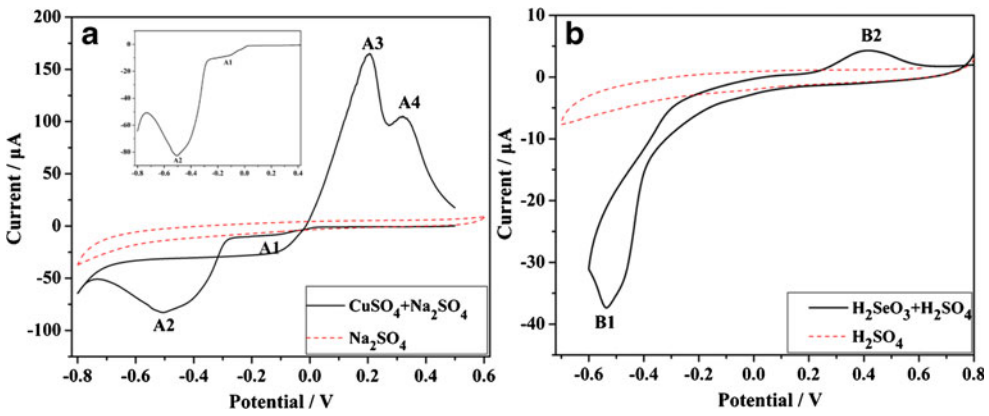

Fig. 1 Cyclic voltammograms: **a** the COOH-CNTs/PI membrane electrode in $CuSO_4$ (pH 4.5). **b** COOH-CNTs/PI electrode in H_2SeO_3 (pH 0.5). The scan rates: 20 mV/s

Table 1 Charge of peak area (Q) and surface coverage (Γ) for different peaks

Peaks	A1	A2	A3	A4
Charge of peak area Q ($\times 10^{-4}$ C)	0.27	4.3	3.2	0.25
Surface coverage Γ ($\times 10^{-9}$ mol/cm^2)	0.46	7.2	5.3	0.42

Results and discussion

Figure 1a shows the cyclic voltammogram for COOH-CNTs/PI membrane electrode in the blank Na_2SO_4 and $CuSO_4$ electrolytic solution. From the patterns, the current basically keeps constant in the Na_2SO_4 solution, and no peaks appear. However, two coupled peaks are observed in the Cu^{2+} containing solution, located at A1 (-0.20 V) and A4 (0.3 V), A2 (-0.50 V) and A3 (0.21 V), respectively. They should be attributed to underpotential and bulk reduction as well as stripping peaks of Cu on membrane substrate; the inset is the amplification part of peaks A1, A2. The relevant electrode reactions are as follows:

$$\mathrm{A1, A2 : Cu^{2+} + 2e \rightarrow Cu} \quad \mathrm{A3, A4 : Cu - 2e \rightarrow Cu^{2+}} \tag{1}$$

According to the Cu peaks in the first cyclic voltammetry (CV) scanning, the surface coverage (mol/cm^2) of the Cu layer on COOH-CNTs/PI membrane can be calculated by the following formula [23]:

$$\Gamma = \frac{Q}{nAF} \tag{2}$$

where Q is the charge of the peak area (coulombs), F is the Faraday constant, n is the number of electrons transferred in the electrode reaction (here n=2), and A refers to the effective electrode area (0.31 cm^2), which were investigated by chronocoulometry method (Fig. S1), indicating that the effective electrode area is larger than the geometric area. The surface coverage (mol/cm^2) results are shown in Table 1. For most of the metal monolayer in UPD studies, the maximum surface coverage is about 2×10^{-9} mol/cm^2 [24], $_{A1}$ and $_{A4}$ values are less than the reported monolayer coverage, when $_{A2}$ and $_{A3}$ are more than the maximum value. Hence, the peaks A1, A4 obtained in Fig. 1a conditions are inferred as the underpotential peaks, while A2, A3 are identified as the bulk peaks.

The cyclic voltammogram of Se on COOH-CNTs/PI membrane electrode with the similar method is shown in Fig. 1b. There is no obvious peak in the blank H_2SO_4 solution, while a reduction peak B1 (-0.52 V) and an oxidation peak B2 (0.40 V) are observed in the H_2SeO_3 solution. They are regarded as the bulk reduction and dissolution peaks. The corresponding electrode reactions were as follows:

$$\begin{aligned} &\mathrm{B1 : H_2SeO_3 + 4H^+ + 4e \rightarrow Se + 3H_2O} \\ &\mathrm{B2 : Se + 3H_2O - 4e \rightarrow H_2SeO_3 + 4H^+} \end{aligned} \tag{3}$$

It has been reported that the deposition of Se does not show classical UPD process, but bulk deposition of Se is so slow that it was required an overpotential to deposit Se [25], thus -0.55 V was chosen as the deposition potential in the experiments.

The amperometric I–t methodology was used to study and deposit the ions on CNTs/PI membrane electrode at constant potential. Because the CV scan of Cu^{2+} on the CNTs/PI electrode showed a surface-limited process analogous to UPD and selenium poor electronic conducting properties, the first deposition layer was a copper UPD layer bonded to substrate. The cycle involved in the work containing the following steps: pouring 10 mL $CuSO_4$ solution into the electrolyzer, depositing at -0.2 V for about 20 s, followed by an additional 30 s of stalling settlement, with no solution flow to allow sufficient time for deposition; Then the electrolyzer was rinsed twice with doubly distilled water and pouring 10 mL H_2SeO_3 solution, again at -0.55 V, depositing for about 15 s, followed by an additional 30 s of stalling settlement, with no solution flow. These steps were intended to form a monolayer of CuSe, following the layers are deposited alternately in the later

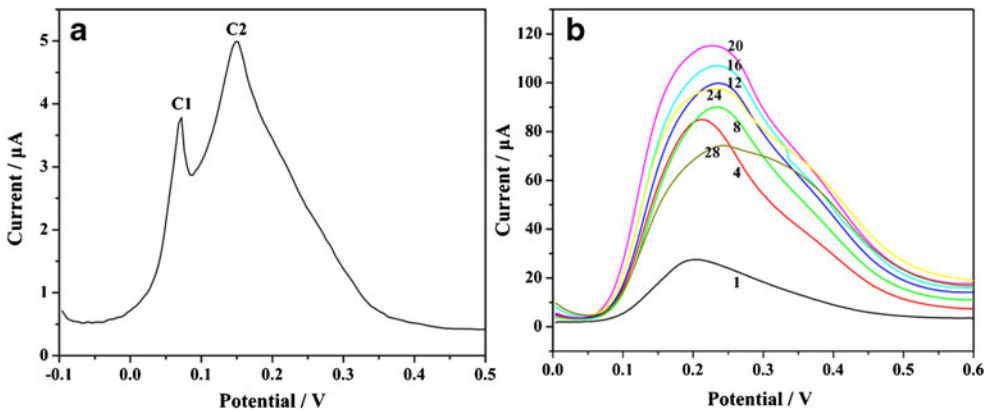

Fig. 2 **a** DPSV of the first copper layer. **b** DPSV of CuSe deposits with different cycles

Table 2 Cu/Se charges and actomic ratios obtained for different cycles

m (cycles)	$Q_{Cu}/10^{-4}$ C	$Q_{Se}/10^{-4}$ C	n_{Cu}/n_{Se}
1	16.26	28.18	4.27/3.71
5	16.66	28.34	4.38/3.73
9	17.52	29.65	4.61/3.90
13	18.58	29.83	4.88/3.92
17	19.18	30.09	5.04/3.96
21	20.52	30.19	5.40/3.97
24	18.50	28.70	4.86/3.77
28	18.40	27.09	4.84/3.56

cycles. The deposition cycle numbers and deposition time were determined according to repeatedly characterization and optimization.

Figure 2a shows stripping voltammograms of copper in 0.1 M H_2SO_4 blank solution from the COOH-MWCNTs/PI electrode. It is observed that copper stripping exhibits two peaks C1 (0.10 V) and C2 (0.20 V), C2 probably corresponds to the dissolution of underpotential layer on the CNTs/PI electrode, while C1 corresponds to the bulk layer deposits on the copper adlayer. They are very similar to the positive peaks shown in Fig. 2a, and the position shifts due to the instability of the copper layer on the electrode. In addition, from the stripping peak shapes and heights, we can see that the C2 is larger than the C1 peak, indicating that the previous deposition process is mainly UPD and partially bulk deposition. Figure 2b presents the differential pulse-stripping voltammogram (DPSV) corresponding to the dissolution of the CuSe deposits in H_2SO_4 solution that are obtained by cycling various times on CNTs/PI electrode. The CuSe deposits exhibit one wide oxidation peak close to 0.2 V, which could be explained for the easy solubility of copper (this comparison can be observed from the CV pattern), and the stripping peaks become wider and higher with increase of the cycle number before the first 23 cycles, accounting for the formation of Cu–Se compound which enhanced the electronic contact area with the working electrode in the earlier stage. However, the current gradually decreases with the cycles accumulating after 24 cycles, since the thickness augment causing the resistance increase, and it appears an unconspicuous peak at about 0.35 V which are caused by selenium dissolving. Table 2 gives the charges and ratios of Cu/Se with different cycles; based on the electric quantity changes, we can draw the similar conclusion with the DPSV results. Hence, the appropriate deposition cycles is determined to be about 24 cycles in this experiment. In addition, due to the easier solubility of copper, the charge ratios of copper and selenium should be controlled to be more than the stoichiometric ratio 1:1, the atomic proportion in Table 2 is calculated by the following equation [26]:

$$n = \frac{Q}{a \times e} \tag{4}$$

where *n* refers to atomic number, *a* is electron transfer number in the reduction process.

For better understanding of the nucleation and growth mechanism of copper on COOH-CNTs/PI substrate, amperometric *I–t* experiments were performed. Generally, two-dimensional (2-D) limiting nucleation mechanism can be described as either instantaneous or progressive: instantaneous nucleation, when the nucleation rate is quick and the maximum current rapidly reaches as soon as the potential is stepped, and progressive nucleation, when the nucleation rate is slow and remained constant. Current density − time (*j–t*) transients about the above two ideal conditions are simply described by the following equations:

$$j_{inst} = at\exp(-bt^2) \tag{5}$$

$$j_{prog} = ct^2\exp(-dt^3) \tag{6}$$

In a potential step experiment *a*, *b*, *c*, and *d* are constants [27]. The experimental data from Fig. 3a were recorded at a potential of -0.2 V, according to the reduced variable plot comparison and the nucleation peculiarities of the two

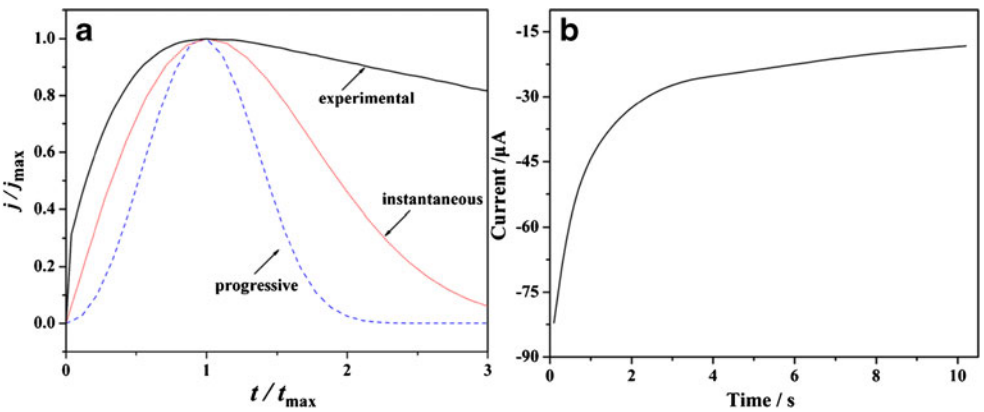

Fig. 3 **a** Reduced variable plot showing fit to instantaneous and progressive nucleation models. **b** Amperometric *I–t* curve of H_2SeO_3 on Cu-covered electrode

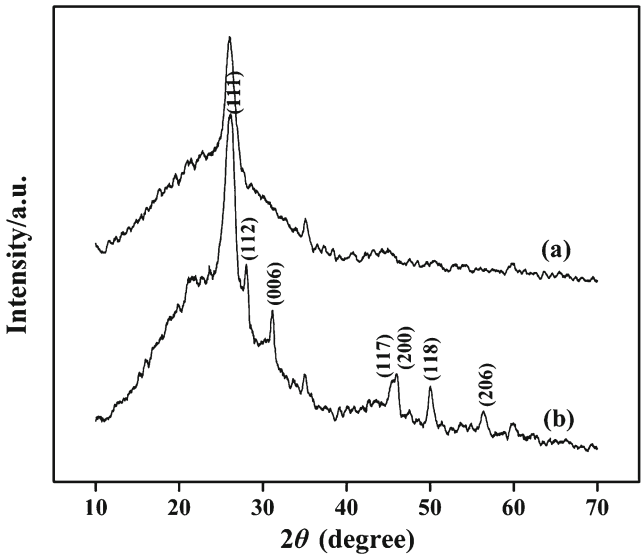

Fig. 4 XRD results of the CuSe thin film

separated means, and the experimental *j–t* transient fits better for the instantaneous behavior. However, a positive deviation of the experimental curve from the ideal condition appeared, and the current increase may be caused by the easy adsorption process of Cu on the COOH-CNTs/PI surface [28]. Hence, the deposition of Cu on COOH-CNTs/PI surface is described as instantaneous nucleation accompanied by adsorption process. The selenium growth on the Cu-covered electrode is considered to be a diffusion control process based on a Cottrell-type current related to the multi-electronic electroreduction of H_2SeO_3 to selenium [29].

Figure 4 shows XRD patterns of COOH-CNTs/PI membrane and CuSe thin films. Both (a) and (b) curves exhibit a typical broad peak that ranges from 15 ° to 30 °, which is attributed to the amorphous glass. As shown in Fig. 2b, the diffraction peaks at 26.30 °, 28.02 °, 31.10 °, 45.33 °, 45.85 °, 49.97 °, and 56.33 ° can be indexed to (111), (112), (006), (117), (200), (118), and (206) planes of orthorhombic CuSe (JCPDS Card, No. 86-1239). The XRD studies reveal the polycrystalline nature of the films, and it can be found out that the preferred orientation of the deposited thin film is at the (112) plane. Furthermore, the XRD pattern shows that the thin film has a single crystal structure of CuSe without secondary structure of other impurities, such as some other composition compounds of copper selenide and single copper or selenium. The highest peak appears at about 26.06 ° owing to the COOH-MWCNTs, which may partially cover CuSe 26.30 ° peak. Furthermore, the peak at approximate 35.19 ° represents a characteristic for the indium tin oxide (ITO) glass substrate [22], and the diffraction peak which appears at near 60 ° both on Fig. 4a and b is assigned to the ITO peak [30].

Figure 5a–e depicts the morphology of different thickness of the as-prepared CuSe crystals via EC-ALD process, along with the substrate. From the inset of Fig. 5a, it can be seen that the product consists of interlaced short virgates with a width varying between 50 and 100 nm as well an uncertain length; they link with each other like little branches, and the overall morphology of the crystals seems rather homogeneous. In addition, Fig. 5a–c exhibit the micrographs of 7, 15, 25 cycles, respectively, the thickness and surface coverage appear to add along with the cycle number increasing, and the interspaces are also reduced. The cross-section image, seen in Fig. 5d, provides a more direct measurement for the thickness of the COOH-CNTs/PI/CuSe material, the thickness of the CNTs/PI membrane measures to

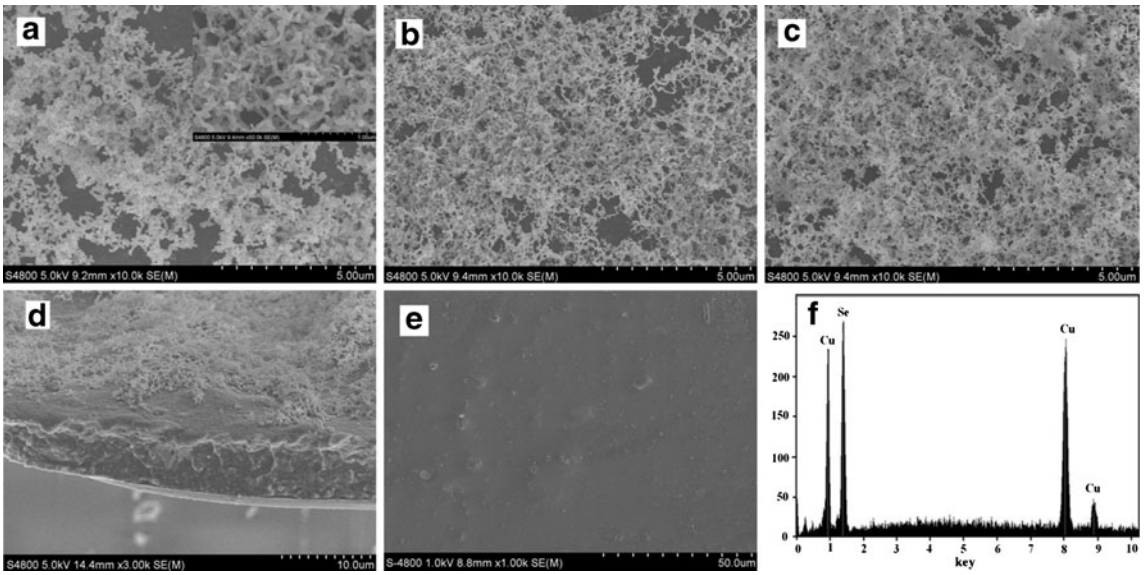

Fig. 5 SEM graphs of CuSe thin films with different cycles: **a** 7 cycles, **b** 15 cycles, **c** 25 cycles, **d** cross-section image of the COOH-CNTs/PI/CuSe material, **e** blank substrate, and **f** EDS pattern of CuSe

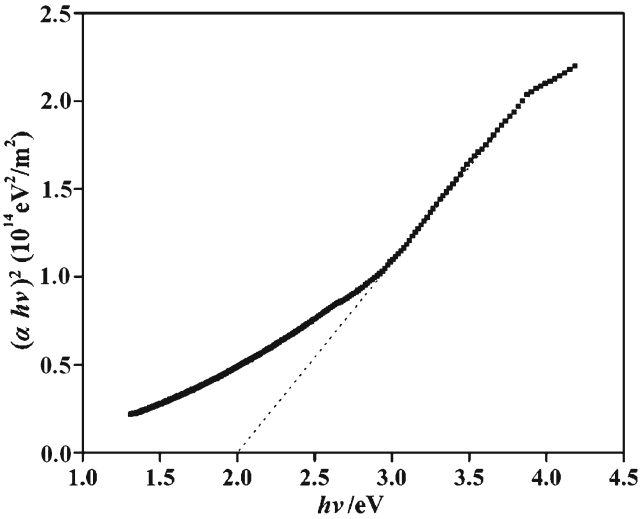

Fig. 6 Plot of $(\alpha h\nu)^2$ vs. $h\nu$ for CuSe thin films

be about 7.69 μm, while that of the CuSe thin film varies from hundreds of nanometer to micrometer. Moreover, the electrodeposits formed on this substrate with a thickness less than micron level showed a good adherence in the experiments. Figure 5e displays the surface of the COOH-CNTs/PI membrane, from the pattern, the MWCNTs can be observed doped in and on the membrane, and it not only increased the conductivity of the composition membrane but also provides a suitable growing condition for the film. The energy-dispersive X-ray spectroscopy (EDS) analyses of the film (Fig. 5f) at different locations of the nanocrystal confirm that an atomic percentage of Cu:Se is close to one. However, because of electrical conductivity difference and surface disparity of every membrane electrode, there were still some problems with reproducibility, such as deposition time and electric current difference for each membrane, and so on. On the other side, by adjusting the deposition time and deposition potential, various ratio compounds are achieved. In addition, it was proved that it formed a single morphology by controlling a certain electric quantity proportion during the experiment, while diverse morphology can be formed by controlling different electric quantity proportions.

The UV–Vis transmission spectrum of the CuSe thin film was explored and the result was shown in Fig. 6. The transmission measurement has recorded over a wavelength range of 250–800 nm. The transmission data are manipulated for calculating the absorption coefficient α dependencies on photon energy. The optical absorption coefficient is determined using the following relation [10]:

$$\alpha = \frac{1}{t}\ln\frac{1}{T} \tag{7}$$

where t is the thickness of the film (400 nm), and T is the transmittance. The band gap can be calculated using the following relation:

$$\alpha h\nu = A(h\nu - E_g)^n \tag{8}$$

where A is a constant, n equals to 1/2 for direct transition [31]. The linear extrapolation to the X-axis ($h\nu$) from the straight part of the curve gives an approximately 2.0 eV bandgap value, which is consistent with the literature [32].

The photo-activity of CuSe thin film was studied by the OCP–time (OCP–t) method through dark and illumination responses. Na_2SO_4 was an ideal electrolyte owing to its stability under chemical conditions. The dark and illumination time intervals were 100 s with xenon lamp. The potential under the condition of the open circuit (V_{OC}) can be described using the following equation [33]:

$$V_{OC} = -kT/eln(1 + bI_0) \tag{9}$$

where I_0 is the light intensity incident upon the film, and b is always a positive number. It generated electron–hole pairs under the illumination, and electrons moved to n-type acceptor when holes moved to p-type acceptor. In the case of p-type semiconductors, the excess holes positively charge the acceptor, namely, -e instead of e in Eq. 9. Hence, V_{OC} was positive and shifted toward a more positive potential upon illumination, as demonstrated in Fig. 7a; when the lamp was turned on, the photo potential increased from 108 to about 124 mV, which illustrates that the as-obtained CuSe thin film is a p-type semiconductor. Figure 7b illustrates the evolution of current vs. time for the CuSe thin film

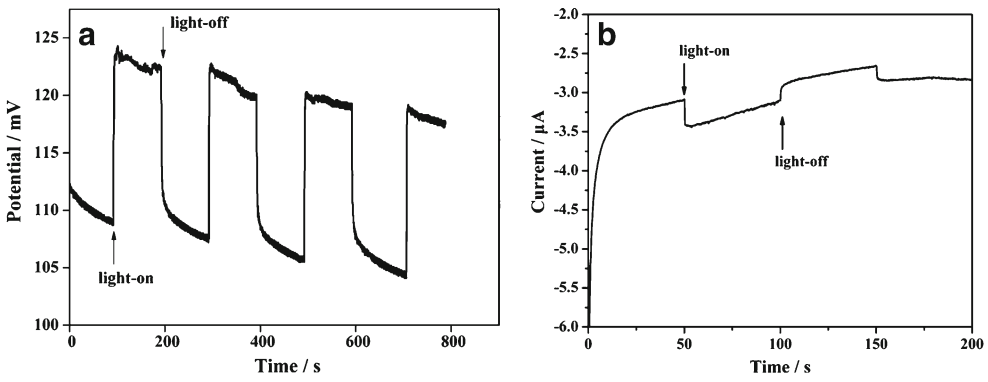

Fig. 7 **a** OCP vs. time. **b** Amperometric current vs. time of CuSe in the dark and under the illumination

maintained at -0.5 V vs. SCE; during successive dark/illumination conditions, the photocurrent change indicates that the samples are p-type [34], which agrees with the OCP results. As a result, this CuSe thin film through electrodeposition on COOH-CNTs/PI membrane (COOH-CNTs/PI/CuSe) is appropriate to serve as the absorbed layer of solar cell.

Conclusions

In our work, the CuSe thin film was successfully fabricated on COOH-CNTs/PI membrane through EC-ALD. By exploring the elements' electrochemical properties by CV and DPV, the optimum deposition conditions of CuSe thin film were determined. The nucleation and growth mechanism of the elements were researched through amperometric *I–t* method, and the nucleation phenomenon of copper fits better for the instantaneous behavior, while the selenium growth on the Cu-covered electrode is considered to be diffusion control process. The XRD data reveal that the preferred orientation of the deposited thin film is at (112) plane. SEM and EDS analyses indicate that the obtained CuSe thin film are short virgate nanostructures, and the average atomic percentage of Cu:Se is close to one. The band gap is calculated to be 2.0 eV, OCP and amperometric *I–t* measurements illustrate CuSe thin film to be p-type semiconductor, and all the results indicate that CuSe thin film fabricated on the COOH-CNTs/PI membrane (COOH-CNTs/PI/CuSe) is appropriate to serve as the solar energy transfer material.

Acknowledgments This work was supported by the National Natural Science Foundation of China (Grant No. 51072073).

References

1. Neyvasagam K, Soundararajan N (2008) Ajaysoni, Okram GS, GanesanV. Phys Status Solidi B 245:77–81
2. Ambade SB, Mane RS, Kale SS, Sonawane SH, Shaikh AV, Han SH (2006) Appl Surf Sci 253:2123–2126
3. Gosavi SR, Deshpande NG, Gudage YG, Sharma R (2008) J Alloys Compd 448:344–348
4. Haram SK, Santhanam KSV, Spallart MN, Clement CL (1992) Mater Res Bull 27:1185–1191
5. Yang YJ, Hu SS (2009) J Solid State Electrochem 13:477–483
6. Bhuse VM, Hankare PP, Garadkar KM, Khomane AS (2003) Mater Chem Phys 80:82–88
7. Gosavi SR, Deshpande NG, Gudage YG, Sharma R (2008) J Alloys Compd 448:344–348
8. Lakshmikumar ST (1994) Sol Energy Mater Sol Cells 32:7–19
9. Abdullaev GB, Aliyarova ZA, Asadov GA (1967) Phys Status Solidi B 21:461–464
10. García VM, Nair PK, Nair MTS (1999) J Cryst Growth 203:113–124
11. Vinod TP, Jin X, Kim J (2011) Mater Res Bull 46:340–344
12. Hankare PP, Khomane AS, Chate PA, Rathod KC, Garadkar KM (2009) J Alloys Compd 469:478–482
13. Haram SK, Santhanam KSV (1994) Thin Solid Films 238:21–26
14. Massaccesi S, Sanchez S, Vedel J (1993) J Electrochem Soc 140:2540–2546
15. Tonejc A, Ogorelec Z, Mestnik B (1975) Appl Cryst 8:375–379
16. Vohl P, Perkins DM, Ellis SG, Addiss RR, Huis W, Noel G (1967) IEEE Trans Electron Dev 14:26–30
17. Okimura H, Matsumae T, Makabe R (1980) Thin Solid Films 71:53–59
18. Malik MA, O'Brien P, Revaprasadu N (1999) Adv Mater 11:1441–1444
19. Kim JY, Kim YG, Stickney JL (2008) Electroanal Chem 621:205–213
20. Mathe MK, Cox SM Jr, Flowers BH, Vaidyanathan R, Pham L, Srisook N, Happek U, Stickney JL (2004) J Cryst Growth 271:55–64
21. Loglio F (2004) InnocentiM, Pezzatini G, Foresti ML. J Electroanal Chem 562:117–125
22. Kou HH, Jiang YM, Li JJ, Yu SJ, Zheng ZX, Wang CM (2011) Electrochim Acta 56:5575–5581
23. Ye WC, Tong H, Wang CM (2005) Microchim Acta 152:85–88
24. Jing F, Tong H, Wang CM (2004) J Solid State Electrochem 8:877–881
25. Huang BM, Lister TE, Stickney JL (1997) Surf Sci 392:27–43
26. Riveros G, Henriquez R, Cordova R, Schrebler R, Dalchiele EA, Gomez H (2001) J Electroanal Chem 504:160–165
27. Shi XZ, Zhang X, Ma CL, Wang CM (2010) J Solid State Electrochem 14:93–99
28. Demir U, Shannon C (1996) Langmuir 12:6091–6097
29. Gomez H, Henriquez R, Schrebler R, Cordova R, Ramirez D, Riveros G, Dalchiele EA (2005) Electrochim Acta 50:1299–1305
30. Tang J, Zheng JJ, Xu W, Tian XC, Lin JH (2011) Acta Phys Chim Sin 27(11):2613–2617
31. Jagminas A, Juskenas R, Gailiute I, Statkuteb G, Tomasiunas R (2006) J Cryst Growth 294:343–348
32. Haram SK, Santhanam KSV (1994) Thin Solid Films 238:21–26
33. Zhang X, Shi XZ, Ye WC, Ma CL, Wang CM (2009) Appl Phys A 94:381–386
34. Guillen C (2002) Herrero. J Sol Energy Mater Sol Cells 73:141–149